MICROCOPY RESOLUTION TEST CHART
NATIONAL BUREAU OF STANDARDS-1963-A

REPORT DOCUMENTATION PAGE

READ INSTRUCTIONS
BEFORE COMPLETING FORM

1. REPORT NUMBER	2. GOVT ACCESSION NO.	3. RECIPIENT'S CATALOG NUMBER
4		

4. TITLE (and Subtitle)	5. TYPE OF REPORT & PERIOD COVERED
INTERFACE CHEMISTRY OF TERNARY SEMICONDUTORS: LOCAL MORPHOLOGY OF THE $Hg_{1-x}Cd_xTe$-Cr INTERFACE	interim; 8/1/84-7/30/86
	6. PERFORMING ORG. REPORT NUMBER

7. AUTHOR(s)	8. CONTRACT OR GRANT NUMBER(s)
A. Franciosi and P. Philip D.J. Peterman (Mc Donnell Douglas Research Labs)	N00014-84-K-0545

9. PERFORMING ORGANIZATION NAME AND ADDRESS	10. PROGRAM ELEMENT, PROJECT, TASK AREA & WORK UNIT NUMBERS
University of Minnesota 1919 University Avenue St. Paul, MN 55104	task NR 372-162

11. CONTROLLING OFFICE NAME AND ADDRESS	12. REPORT DATE
Office of Naval Research Electronics Division (K. Hathaway)	10/15/85
	13. NUMBER OF PAGES
Department of the Navy, Arlington, VA 22217	27

14. MONITORING AGENCY NAME & ADDRESS(if different from Controlling Office)	15. SECURITY CLASS. (of this report)
	unclassified
	15a. DECLASSIFICATION/DOWNGRADING SCHEDULE

16. DISTRIBUTION STATEMENT (of this Report)

Approved for public release; unlimited distribution

17. DISTRIBUTION STATEMENT (of the abstract entered in Block 20, if different from Report)

DTIC
ELECTE
NOV.1 4 1985

A

18. SUPPLEMENTARY NOTES

to be published in Physical Review B32

19. KEY WORDS (Continue on reverse side if necessary and identify by block number)

Interface reactivity; Metal-semiconductor interfaces

20. ABSTRACT (Continue on reverse side if necessary and identify by block number)

Synchrotron Radiation Photoemission studies of interfaces prepared in situ on cleaved substrates show atomic interdiffusion with Cr/Hg and Cr/Cd exchange reactions taking place at room temperature for Cr coverages less than 2Å. Correspondingly, dissociated Te is released at the surface. A subsurface region 10-13 Å thick is formed in which Cr atoms replace all of the Hg atoms and at least 20% of the Cd atoms. Below this subsurface the semiconductor maintains the bulk stoichiometry and the initial surface band bending.

DD FORM 1473 EDITION OF 1 NOV 65 IS OBSOLETE
1 JAN 73
S/N 0102-LF-014-6601

unclassified
SECURITY CLASSIFICATION OF THIS PAGE (When Data Entered)

U M

UNIVERSITY OF MINNESOTA
TWIN CITIES

Department of Chemical Engineering and Materials Science
151 Amundson Hall
421 Washington Avenue S.E.
Minneapolis, Minnesota 55455
(612) 373-2300

October 15, 1985

Dr. K. Hathaway
Office of Naval Research
Electronics Division
Department of the Navy
Arlington, VA 22217

Dear Dr. Hathaway:

Enclosed please find a preprint of the article "Interface Chemistry of Ternary Semiconductors: Local Morphology of the $Hg_{1-x}Cd_xTe(110)$-Cr Interface", that we recently submitted to Physical Review. In the paper we acknowledge the support of the Office of Naval Research, that is funding our research under grant N00014-84-K-0545 "Microscopic Control of Semiconductor Interface Reactivity". The paper is soon to appear in Physical Review B32.

In this paper we focus on the HgCdTe-Cr interface reactions, that is of interest to us because of the potential role of Cr in controling the reactivity of the HgCdTe surface. In a number of previous papers we have shown that Cr overlayers can control the reactivity of Si and GaAs surfaces (see A. Franciosi et al., J. Vac. Sci. Technol. A3, 933 (1985) for reaction with activated oxygen, acting as a relatively powerful catalyst. This effect appears related to the local morphology of the Cr-semiconductor interface and to the chemistry of the transition metal. Semiconductor of the II-VI family are known to exhibit substantial ionic character in the bonding and to give rise to strong exchange reactions following metal deposition. It is of great interest to explore how the catalytic activity of a metal overlayers is affected by such a different interface morphology. In this paper we lay a background for such a study by characterizing the local interface morphology of the HgCdTe-Cr system.

We have chosen HgCdTe alloys for their II-VI character and for their technological interest. Such materials have widespread application for infrared detectors in the 8-12 µm spectral range, and the chemistry of their interfaces with metals is largely unknown. Our results show that the local interface morphology is surprisingly more complex compared to those reported for the HgCdTe-Al and HgCdTe-Au interfaces. Cr/Hg and Cr/Cd exchange reactions take place at room temperature with the formation of a 10-13 Å thick subsurface layer virtually completely depleted of mercury. This dramatic reaction has no influence on the Schottky barrier, in contrast with the assumptions of all existing models of HgCdTe-metal junction behavior.

Yours sincerely

Alfonso Franciosi
Assistant Professor

INTERFACE CHEMISTRY OF TERNARY SEMICONDUCTORS:
LOCAL MORPHOLOGY OF THE $Hg_{1-x}Cd_xTe$ (110)-CR INTERFACE

A. Franciosi and P. Philip
Department of Chemical Engineering and Materials Science
University of Minnesota, Minneapolis, MN 55455

and
D.J. Peterman
McDonnell Douglas Research Laboratories
St. Louis, MO 63166

ABSTRACT

Synchrotron radiation photoemission studies of interfaces prepared in situ on cleaved substrates show atomic interdiffusion with Cr/Hg and Cr/Cd exchange reactions taking place at room temperature for Cr coverages less than 2Å. Correspondingly, dissociated Te is released at the surface. A subsurface region 10-13 Å thick is formed in which Cr atoms replace all of the Hg atoms and at least 20% of the Cd atoms. Below this subsurface the semiconductor maintains the bulk stoichiometry and the initial surface band bending.

Very little is known about the interface chemistry of ternary semiconductor alloys. The results available on compound semiconductors[1-2] can be extrapolated only in part to ternary alloys, where the interplay of two different kinds of chemical bonding can substantially change the character and stability of each bond with respect to those of the binary parent compounds. Mercury-Cadmium-Telluride is probably the ternary semiconductor most studied in recent years because of its widespread application for infrared detectors in the 8-14 μm spectral range. This material poses a number of intriguing fundamental and technological problems that only now are starting to be addressed. As a ternary semiconductor alloy formed from parent compounds of very different stability, this material easily sustains composition variations. It has also been recently recognized that the interplay of ionicity and metallicity in the two kinds of chemical bonding that coexist in the matrix further weakens[3,4] one bond (Hg-Te) relative to the other (Cd-Te) causing lattice, surface and interface instabilities in the alloy.[5] For example, dramatic composition variations have been observed in $Hg_{1-x}Cd_xTe$ as a result of processes as diverse as mechanical damage,[6-7] oxidation,[8] and metal deposition.[9-10] A detailed understanding of the interface chemistry and physics of this material requires a systematic analysis of variations in local stoichiometry, Schottky barrier height and interface width.

Pioneering photoemission studies have recently clarified the nature of chemical bonding in the bulk alloy,[11,12] and related the Schottky barrier height for the $Hg_{1-x}Cd_xTe(110)$ - Al[10] and $Hg_{1-x}Cd_xTe(110)$ - Au[13] interfaces to the local composition of the semiconductor surface layer. In this paper we focus on the chemistry of $Hg_{1-x}Cd_xTe$-refractory metal interfaces, which represent a new class of technologically important junctions that are largely unexplored. We have performed synchrotron radiation photoemission studies of the $Hg_{1-x}Cd_xTe(110)$-Cr interface formed in situ. Results concerning the connection between Schottky barrier height and the changes in semiconductor surface composition have been presented earlier.[14] Here we describe the local morphology of the interface region in detail and relate the interface electronic properties to the local chemistry of the material.

Experimental

Single crystals of $Hg_{1-x}Cd_xTe$ were prepared at McDonnell Douglas using a modified Bridgman method. Several oriented (110) posts (3x3x15 mm^3) were cut from the center of the cylindrical portion of a boule. Samples cut from each end of the cylinder showed an identical energy gap of 0.175 ± 0.01 eV and p-type conductivity with a room temperature carrier concentration of $2x10^{16}cm^{-3}$, as determined from infrared transmission and Hall effect measurements, respectively. The sample composition, deduced from the bandgap measurements[15] was x=0.22 ± 0.01. The posts were loaded into the photoelectron spectometer through a special fast-insertion device, thus allowing an operating pressure $<5x10^{-11}$ torr while avoiding sample exposure to high temperature. The posts were cleaved in situ with varying degrees of success at obtaining mirror-like surfaces. The photoemission measurements were performed by positioning the samples at the common focus of the monochromatic photon beam and a commercial double pass cylindrical mirror analyzer. Photoelectron energy distribution curves (EDC's) were recorded for 40<hv<140 eV using a "grasshopper" grazing incidence monochromator and synchrotron radiation from the 240 MeV electron storage ring, Tantalus, at the Synchrotron Radiation Center of the University of Wisconsin-Madison. The overall energy resolution (electrons plus photons) ranged from 0.4-0.7 eV for hv<100 eV to about 0.8-1.0 eV for the high photon energy studies (Te 4d and Cr 3p cores at hv=110 eV). The interfaces were prepared in situ by direct Cr sublimation from a W coil and the metal coverage was monitored using a quartz thickness monitor.

RESULTS

A. Valence states

The experimental results are organized in two series of figures. Figures 1-4 show valence band spectra for the clean and Cr-covered $Hg_{1-x}Cd_xTe$ surfaces, Figs. 5-10 summarize results for the core level emission. In the photon energy range available to us we were able to monitor the evolution of the Hg 5d, Cd 4d, Te 4d and Cr 3p core levels as a function of metal coverage, gaining information on the relative

concentration and on the local chemical environment of each atomic species present in the interface region.

In Fig. 1 we show representative energy distribution curves (EDC's) for the valence band emission of the cleaved $Hg_{1-x}Cd_xTe$ surface. The zero of the binding energy scale corresponds to the spectrometer Fermi level as derived from the Fermi level cut-off of the high-Cr-coverage EDC's. The spectra have been approximately normalized to the main emission features, and are given in arbitrary units. The EDC's show good qualitative agreement with the results of Silberman et al.[11] and exhibit a Te-p-derived density-of-states feature within 3.5 - eV of the Fermi level E_F, and a second structure between 4 and 7 eV derived primarily from unresolved Cd-s and Hg-s features which reflect the metal s-chalcogenide p hybridization responsible for the stability of the alloy.[16]

The emission features between 8 and 12 eV correspond to the Hg 5d and Cd 4d core levels. Deconvolution of two doublets was performed using the experimental lineshape of the Hg 5d and Cd 4d levels obtained from cleaved HgSe and CdSe samples. As an example, the result of the decomposition for the clean surface is shown in the top section of Fig. 6. All cleaves resulted in identical Hg/Cd/Te ratios (as determined by the ratios of the Hg 5d, Cd 4d and Te 4d integrated emissions) irrespective of cleave quality, and no-time dependent change of the surface composition was observed after cleaving. From the EDC's of Fig. 1 it is possible to estimate the position of the valence band maximum, E_v, by linearly extrapolating the valence band edge at low binding energy. From all cleaves we obtained $E_v = 0.49 \pm 0.15$ which, when compared with the measured bulk band gap of only 0.175±0.01 eV, indicates a strongly inverted (n-type) character for the near surface region.

The effect of Cr deposition on the valence band emission is shown in Fig. 2 for hv=60 eV. The bottom-most spectrum is the clean surface spectrum while EDC's displaced upwards correspond to increasing Cr coverages, Θ, and are given in relative units. Two effects are clearly evident in Fig. 2. First, emission from the Cr 3d states quickly dominates the valence band spectra within 3 eV of E_F. Second, the Hg-derived emission decreases dramatically and is almost negligible at

concentration and on the local chemical environment of each atomic species present in the interface region.

In Fig. 1 we show representative energy distribution curves (EDC's) for the valence band emission of the cleaved $Hg_{1-x}Cd_xTe$ surface. The zero of the binding energy scale corresponds to the spectrometer Fermi level as derived from the Fermi level cut-off of the high-Cr-coverage EDC's. The spectra have been approximately normalized to the main emission features, and are given in arbitrary units. The EDC's show good qualitative agreement with the results of Silberman et al.[11] and exhibit a Te-p-derived density-of-states feature within 3.5 - eV of the Fermi level E_F, and a second structure between 4 and 7 eV derived primarily from unresolved Cd-s and Hg-s features which reflect the metal s-chalcogenide p hybridization responsible for the stability of the alloy.[16]

The emission features between 8 and 12 eV correspond to the Hg 5d and Cd 4d core levels. Deconvolution of two doublets was performed using the experimental lineshape of the Hg 5d and Cd 4d levels obtained from cleaved HgSe and CdSe samples. As an example, the result of the decomposition for the clean surface is shown in the top section of Fig. 6. All cleaves resulted in identical Hg/Cd/Te ratios (as determined by the ratios of the Hg 5d, Cd 4d and Te 4d integrated emissions) irrespective of cleave quality, and no-time dependent change of the surface composition was observed after cleaving. From the EDC's of Fig. 1 it is possible to estimate the position of the valence band maximum, E_v, by linearly extrapolating the valence band edge at low binding energy. From all cleaves we obtained $E_v=0.49\pm0.15$ which, when compared with the measured bulk band gap of only 0.175±0.01 eV, indicates a strongly inverted (n-type) character for the near surface region.

The effect of Cr deposition on the valence band emission is shown in Fig. 2 for hv=60 eV. The bottom-most spectrum is the clean surface spectrum while EDC's displaced upwards correspond to increasing Cr coverages, Θ, and are given in relative units. Two effects are clearly evident in Fig. 2. First, emission from the Cr 3d states quickly dominates the valence band spectra within 3 eV of E_F. Second, the Hg-derived emission decreases dramatically and is almost negligible at

Θ~3 Å. These two trends are shown in more detail in Figs. 3 and 5 where we have plotted, in an expanded scale, the valence band emission within 9 eV of E_F and the Hg 5d - Cd 4d core emission, respectively. In Fig. 3 we see that initial Cr deposition gives rise to increased valence emission within 2 eV of E_F, and to a "tailing" of valence states at E_F. A true Fermi level cut-off, however, cannot be seen until Θ~3 Å. At this point, the 3d emission gives rise to a main emission feature centered 1.3 - 1.4 eV below E_F which is relatively sharp (full width at half maximum FWHM ~2,7-2.8 eV) compared to the more bulk-like Cr emission at Θ=25Å. Very little change of the valence states is observed for 10<Θ<25 yet there are several relevant differences compared to bulk Cr. This is shown in Fig. 4 where the topmost spectrum (solid line) was obtained from a 250 Å thick Cr film evaporated on oxidized Ta, and the bottom-most spectrum from the $Hg_{1-x}Cd_xTe$ interface with Θ=25 Å (coverage corresponding to over 30 monolayers, taking 1 ml = 6.8×10^{14} atoms/cm^2=total surface atomic density for $Hg_{1-x}Cd_xTe(110)$). The main differences we note (tic marks) are shift of the main 3d feature by 0.2 eV to higher binding energy, increased emission within 1 eV of the Fermi level, and a rather broad density-of-states feature centered 12.5 eV below E_F.

B. Core Emission

Fig. 5 shows the evolution of the Hg 5d and Cd 4d core lineshape in the 0<Θ<3 Å coverage range for hv=60 eV. The spectra were obtained from the EDC's of Fig. 2 after subtraction of a smooth secondary electron background and are given in relative units. The vertical dashed lines mark the position of the Hg $5d_{5/2}$, Hg $5d_{3/2}$ and Cd $4d_{5/2}$ levels after deconvolution (see top section of Fig. 6). Emission from all cores appears strongly attenuated even at low metal coverages (note the scale factors in Fig. 5). Furthermore, the Hg-to-Cd ratio decreases dramatically with increasing metal coverage. The binding energy of the Hg 5d cores remains unchanged as a function of metal coverage within experimental uncertainty (~0.1 eV). For the Cd cores, our data show constant binding energy for Θ<1 Å, and suggest a sharp 0.3-0.4 eV binding energy increase for 1Å<Θ<3Å.[17]

To examine quantitatively the surface concentration of Hg and Cd as a function of coverage, the two doublets were deconvolved as sketched in the top section of Fig. 6. The total integrated intensity of each doublet at a given coverage Θ was normalized to the zero-coverage emission intensity, and is shown in a semi-logarithmic plot in the lower section of Fig. 6. The solid lines correspond to an exponential attenuation of the core emission. The resulting attenuation lengths[18] are 0.7Å and 1.7Å, respectively, for the Hg 5d and Cd 4d cores. The attenuation of the Cd and especially of the Hg core emission is far more rapid than can be reasonably expected from an escape-depth-driven mechanism, where an attenuation length of 4-5Å would be expected.[19]

EDC's for the Te 4d core emission at $h\nu$=110 eV and $h\nu$=53 eV are shown (solid lines) in Fig. 7 and 8, respectively. The spectra appear all approximately normalized to the main emission feature to emphasize the lineshape changes. The EDC's (solid lines) in Fig. 7 show that the sharp experimental 4d lineshape for the clean surface is broadened asymmetrically at Θ=1.5 and 3.0 and shifted to lower binding energy. For Θ>10, however, the line width decreases again while the doublet is shifted to higher binding energy. These non-monotonic trends can be explained by the existence of two 4d lines, shifted by 0.5 eV from each other, and with a coverage-dependent relative intensity. To fit the experimental spectra, we used two 4d lineshapes obtained from the clean surface emission and, as fitting parameters, the binding energy and relative intensity of the two 4d components. The result of the fit is shown in Fig. 7 by a short-dashed line. The fit is remarkably good, and the experimental lineshape appear to be composed of a low binding energy doublet (Te 4d I) that dominates at low coverage, and by a new high-binding-energy component (Te 4d II) 0.45 eV above the main line that grows as a result of Cr deposition, and becomes the dominant feature at Θ=10Å. At coverages greater than 10Å the Cr 3p core contribution, at a binding energy of about 42 eV, is not negligible, even for $h\nu$=110 eV, and the fit cannot be obtained by simply superimposing two Te 4d lines. This is demonstrated by the results at $h\nu$=53 eV in Fig. 8. At photon energies close to the photoemission threshold, one expects the centrifugal barrier to emphasize the Cr 3p

as compared to the Te 4d emissions in our EDC's. The experimental
lineshapes in Fig. 8 (solid line) reflect, in fact, the superposition
of the two 4d lines and a Cr 3p line (dotted line). Again, to reduce
the number of fitting parameters, we used an experimental Cr 3p
lineshape determined from evaporated Cr films, and we let the binding
energy and intensity of this line to be the additional fitting
parameters. The results (shown with short-dashed lines in Fig. 8) were
extremely rewarding. We emphasize that the results of the fitting at
hv=53 eV confirm those at hv=110 eV since the binding energy of each Te
4d line was identical, within experimental uncertainty, in the two
cases. The binding energy of each Te component and of the Cr 3p line
is shown in Fig. 9. The Cr 3p emission appears initially at constant
binding energy (for $\theta < 3\text{Å}$) and then shifts towards higher binding
energy. The final binding energy at high metal coverage appears close
to the bulk Cr value (41.95 ± 0.1 eV versus 42.22 ± 0.15 eV). The
binding energy of the Te II component remains relatively unchanged as a
function of coverage, with at most a gradual 0.1 eV decrease in the
whole coverage range. The Te I component, that starts at the clean
surface position, shifts rigidly 0.25 eV to lower binding energy during
initial metal deposition ($\theta < 2$) and then remains unchanged. The
integrated intensity of each Te 4d component is plotted in Fig. 10 as a
function of metal coverage for hv=53 eV. The overall Te 4d emission
(component I plus component II) is compared in the lower part of Fig. 6
(full squares) with the Cd 4d and Hg 5d core emission. It is readily
seen from Fig. 6, that the attenuation of the Te 4d core emission is
relatively small compared to that of the Cd and Hg core emissions.
This is because while the Te I component exponentially decrease in
intensity (lower section, Fig. 10) the Te II component (upper section,
Fig. 10) grows dramatically during deposition of the first two
monolayers. The results at hv=110 eV are similar, except for the
higher saturation value of the Te II emission, about 60-80% of the
clean surface emission as opposed to 40%.

Discussion

A. Composition Variations

The results of Figs. 1-10, and in particular, of Figs. 2, 3, 9 and 10, suggest that different processes occur at the interface in the low coverage range $0 < \Theta < 2$, and in the high coverage range $\Theta > 2$ Å. In Fig. 6, we showed that dramatic changes in the relative Hg/Te and Hg/Cd concentrations at the surface occur upon Cr deposition at low coverage. For 2Å Cr coverage the Hg 5d core level emission is reduced to about 4% of the initial value, the Cd 4d emission to about 30%, while the overall Te 4d emission remains near the clean surface value (100%). The reduction of the Hg signal is explained by a combination of three experimental observations: a) Hg-depletion of the semiconductor surface layer; b) layer-by-layer Cr coverage of the reacted surface; and c) Te outdiffusion at the surface of the Cr film. The analysis of the Te 4d lineshape gives us a guideline to interpret the remaining experimental results. Figs. 7 and 8 show that two well-defined chemical environments exist for the Te atoms at the surface. The Te I environment is related to the bulk semiconductor $Hg_{0.78}Cd_{0.22}Te$ environment, as indicated by the Te 4d I binding energy which starts at the clean surface value (and then shifts rigidly to lower binding energy (Fig. 9)). The Te II environment is sharply different from the initial semiconductor environment, as indicated by the 0.4-0.5 eV increase in 4d binding energy, which varies very little with further metal deposition (Fig. 9). The intensities of the Te I and Te II components (Fig. 10) exhibit sharply different coverage dependencies. The Te II component increases dramatically at low coverage ($\Theta < 2$Å), with a suggestive inverse relationship to the sharp decrease of the Hg 5d emission (Fig. 6). At higher coverage it saturates to a constant limit of about 40% of the initial overall Te emission ($h\nu = 53$ eV). The saturation value at $h\nu = 110$ eV is, instead, about 70%. Because of the shorter escape depth at $h\nu = 110$ eV, this last point clearly indicates the surface character of the Te 4d II emission. It is possible to roughly estimate the amount of Te at the film surface by calculating the thickness d of a Te layer which would give rise to the same 4d emission intensity observed at the highest metal coverage. Assuming

the Te photoionization cross section to be similar in the semiconductor and in the Te II environment, one obtains

$$\frac{I^{II}_{Te}\,(\Theta)}{I_{Te}\,(o)}\,\Bigg|\,_{\to\infty} \simeq 1-e^{-d/L}$$

where L is the photoelectron escape depth (L≃4Å at hν=110 eV and L≃8Å at hν=53 eV[19]). For both hν=53 eV and hν=110 eV we obtain d≃3 Å i.e. about 1.3 monolayers, in terms of the Te surface atomic density on the $Hg_{0.78}Cd_{0.22}Te$ (110) surface. The Te II emission is therefore localized in a relatively thin surface layer of the deposited film. Further information on the chemical environment of the Te II component can be obtained from the high coverage Cr 3p (Fig. 9) and valence band (Fig. 4) results. At high metal coverages (Θ~25) the Te I emission does not contribute appreciably (Fig. 10) and the results of Fig. 4 and 9 reflect the interaction of the Te II species with the top layers of the Cr film. Correspondingly, the Te 4d II binding energy (0.4 - 0.5 eV above the initial 4d substrate emission) is consistent with the "elemental Te" core binding energies reported in Refs. 20 and 21, and the Cr 3p binding energy is close to the elemental Cr 3p value. This suggests a relatively small Cr-Te interaction for the Te II environment. The valence band results of Fig. 4 are qualitatively consistent with such a picture. An "elemental Te" valence emission is expected to show[22] a 5s emission feature peaked some 12 eV below the valence band edge and a leading emission feature within 1.5 eV of the valence band edge, deriving from the Te lone-pair p-electrons. Fig. 4 shows that the high coverage valence band spectra exhibit indeed a 12.5 eV broad emission feature absent in Cr and increased emission within 1 eV from E_F. We therefore suggest that the Te II species that are released at the surface during the early stages of interface formation reflect mostly an elemental Te environment.

The sharp decrease of the Hg 5d emission (Fig. 6) for Θ<2 cannot be explained simply by layer-by-layer coverage of the HgCdTe substrate, even if one takes into account the formation of an additional Te II surface layer. Hg has to migrate away from the surface layer. Since

the binding energy of the Hg 5d cores (Fig. 5) remains unchanged, this process is likely to produce a surface layer completely depleted of Hg rather than a layer with graded Hg content. In the first case one would expect the residual Hg emission to come from deeper in the solid and to reflect a relatively unperturbed HgCdTe environment. In the second case one would expect, instead, several inequivalent environments for Hg atoms within the experimental sampling depth, with consequent broadening and shift of the Hg 5d cores, in contrast with the results of Fig. 5. The residual 4% Hg 5d emission observed in Fig. 5 at Θ=2 Å, is consistent with complete Hg-depletion of a 13-16 Å thick surface layer.[23] The residual Hg core emission would then reflect the stoichiometric HgCdTe semiconductor below this layer. The Te emission, instead reflects both the dissociated species at the surface of the evaporated film (Te II) and the reacted Te I species in the subsurface layer (see next section). We emphasize that at Θ=2 only an estimated 10-15% of the Te I emission (hν=53 eV) originates from regions of the semiconductor deep enough in the solid so to reflect the stoichiometric situation.

B. Exchange Reactions

In the lower part of Fig. 10 we show that the intensity of the Te I core emission (hν=53 eV) decreases to about 70% of its initial value for Θ~2Å and, at higher metal coverages, follows an exponential behavior with attenuation length of 7-8Å. Since this value is consistent, within experimental uncertainty, with the photoelectron escape depth, we identify the Te I component as Te subsurface emission. Our results show, therefore, no evidence of Cr-Te interdiffusion at high metal coverages (Θ>2). For Θ<2, the interpretation of the results of Fig. 10 is complicated by the outdiffusion of Te II species and by Hg-migration away from the surface. For Θ~2 we note that the observed Te I intensity (70%) is consistent with the attenuation expected from the Te II layer alone, as if the Cr did not contribute to the attenuation. This, together with the binding energy change of the Te 4d I cores observed for Θ<2, argues for substrate-overlayer interdiffusion in this coverage range. The Hg-depletion would be then related to the replacement of Hg-Te bonds with the more stable Cr-Te

bonds. An independent check of this hypothesis can be obtained by comparing the observed attenuation of the Hg emission with the Cr atomic density. At $\Theta = 2$ we have observed a 13-16Å depletion layer at the film surface. The Te II surface layer accounts for ~3 Å. The remaining 10-13 Å subsurface layer contains $\approx 1.2-1.5 \times 10^{15}$ Hg-sites/cm^2. At $\Theta \approx 2$ the Cr surface density is $\approx 1.67 \times 10^{15}$ atoms/cm^2. Therefore, the Hg attenuation is roughly consistent with a one-to-one exchange reaction between Cr and Hg atoms, followed by diffusion of the dissociated Hg away from the surface and subsurface layer.

The core binding energy results are more difficult to interpret due to the presence of a number of semiconducting and metallic species of rapidly varying composition. During the Hg-Cr exchange reaction the Te 4d I core shifts by about 0.25 eV to lower binding energy. This shift could reflect a net charge transfer to the Te atom because of the reduced Cr electronegativity compared to that of Hg. The rigid shift of the Te I core level and the fact that it is independent of the experimental sampling depth (4Å<L<8Å for 110 eV>hν>53 eV) further confirms the picture of a Cr-Te reacted subsurface layer with a depth which is larger than L. The Cr 3p binding energy (Fig. 9) appears constant in the first interface formation stage ($\Theta<2$), in agreement with a one-to-one exchange picture that yields a similar local environment for all Cr atoms in the subsurface region. After the reaction is completed, the Cr cores shift toward the bulk Cr position, as expected since no interdiffusion takes place for $\Theta>2$ Å. The Cr 3p binding energy for $\Theta\sim2$ Å is 0.5±0.1 eV less than that for the final "metallic" position. This would seem to argue against a net charge transfer from Cr to Te atoms during the exchange reaction. We emphasize, however, that the observed "chemical shift" needs not be related in an elementary way to the actual charge transfer[24]. Furthermore, for Cr atoms isolated in a non-metallic matrix, as appears to be the case for $\Theta<2$ Å (Fig. 3), the binding energy should be measured from the vacuum level and would reflect the effective work function of the subsurface and surface species.[25] If we take, for example, the high coverage Cr 3p and Te 4d II binding energy as representative of the elemental Cr 3p and Te 4d emission, then at $\Theta\sim2$ Å both the Cr 3p core level and Te 4d I core levels exhibit an analogous

~0.5 eV shift to lower binding energy relative to the elemental state, with no clear indication of net charge transfer in any direction.

Exchange reactions between metal overlayers and semiconductor cations have been observed in II-VI semiconductors such as CdSe and CdTe.[1,2] In these materials dissociated Cd has been reported in the interface region and its presence has been related to the production of ohmic contacts onto the semiconductor surface. These dissociated Cd species are characterized by a 0.5-0.6 eV _lower_ 4d binding energy compared to Cd in the II-VI semiconductor environment.[26] Our results show that the Cd emission from the HgCdTe-Cr interface decreases more slowly in intensity than the Hg emission, and that the binding energy of the Cd 4d cores seems to increase by about 0.3 eV at $\Theta=3$. Therefore, while the subsurface region does contain a substantial amount of Cd, these atoms appear to be neither bulk-HgCdTe-like nor dissociated. A possible explanation is that the Cd atoms in the subsurface region interact with Cr when Cr replaces the neighboring Hg atoms with a charge transfer from Cd to Cr. Due to the higher stability of the Cd-Te bond as compared to the Hg-Te bond, the probability of Cr replacing Cd in the structure is smaller. If the exchange occurs, Cd atoms must migrate away from the subsurface region since we have no evidence of dissociated Cd within the experimental sampling depth. Both Cd and Hg, in fact, exhibit large diffusion coefficients in $Hg_{1-x}Cd_xTe$ at room temperature.[6] From the reduction in intensity of the Cd emission at $\Theta \sim 2$ we can estimate a lower limit for this Cr-induced Cd-deficiency in the subsurface layer of $0.7-1.0 \times 10^{14}$ atoms/cm^2. This would be consistent with the difference between the Cr surface concentration at $\Theta \sim 2$ of 1.67×10^{15} atoms/cm^2 and the available Hg sites in the subsurface layer ($\sim 1.2-1.5 \times 10^{15}$ atoms/cm^2). In this picture, upon metal deposition Cr atoms would replace all of the Hg atoms and at least 20% of the Cd atoms in the subsurface layer. The model implies that the residual Hg 5d emission seen at $\Theta \approx 2$ Å is representative of the bulk semiconductor underlying the subsurface layer and its binding energy reflects the bulk stoichiometry and the near-surface band bending.[14] Systematic investigation with variable escape depth and high resolution for the Cd 4d cores is necessary to further verify the validity of this model.

Conclusions

The local morphology of the $Hg_{1-x}Cd_xTe(110)$-Cr interface is rather complex compared to those reported for the $Hg_{1-x}Cd_xTe$-Al and $Hg_{1-x}Cd_xTe$-Au interfaces. A description of this morphology was possible only through systematic studies of the core emission from each of the chemical species involved and, in particular, through careful lineshape analysis of the Te 4d emission. Valence and core results are consistent with a first interface formation stage ($\Theta<2$) where Cr replaces all of the Hg atoms and at least 20% of the Cd atoms in a 10-13 Å thick layer of the semiconductor. At the same time Te atoms are released from the semiconductor and form an elemental Te layer at the surface. When the exchange reaction is completed ($\Theta\sim2$Å), about 1.2-1.5×10^{15} Hg atoms in the subsurface layer have been replaced by Cr atoms. Further Cr deposition gives rise to a metallic Cr film covered by the dissociated Te species produced during the first stage of interface reaction (~1.3 monolayers). The typical high coverage interface morphology consists, therefore, of an elemental Te surface, a metallic Cr film, a Hg-depleted 10-13Å subsurface region where Cr-Te and Cd-Te bonds coexist, on top of the ternary semiconductor bulk. The Hg core emission from the underlying bulk remains at a constant binding energy indicating that the bulk environment and the semiconductor band bending[14] remain unchanged beneath the surface and subsurface layers.

References

1. For an extensive review see: L.J. Brillson, Surf. Sci. Rep. 2, 123 (1982).

2. G. Margaritondo and A. Franciosi, Ann. Rev. Mater. Sci. 14, 67 (1984) and references therein.

3. W.A. Harrison, J. Vac. Sci. Technol. A1, 1672 (1983).

4. A.-B. Chen, A. Sher, W.E. Spicer, J. Vac. Sci. Technol. A1, 1675 (1983).

5. W.E. Spicer, J.A. Silberman, I. Lindau, A.-B. Chen, A. Sher, and J.A. Wilson, J. Vac. Sci. Technol. A1, 1735 (1983).

6. H.M. Nitz, O. Ganschow, V. Kaiser, L. Wiedmann, and A. Benninghoven, Surf. Sci. 104, 365 (1981).

7. A. Lastras-Martinez, V. Lee, J. Zehnder, and P.M. Raccah, J. Vac. Sci. Technol. 21, 157 (1982).

8. J.A. Silberman, D. Laser, I. Lindau, and W.E. Spicer, J. Vac. Sci. Technol. A1, 1706 (1983).

9. G.D. Davis, N.E. Byer, R.R. Daniels, and G. Margaritondo, J. Vac. Sci. Technol. A1, 1706 (1983).

10. R.R. Daniels, G. Margaritondo, G.D. Davis, and N.E. Byer, Appl. Phys. Lett. 42, 50 (1983).

11. J.A. Silberman, P. Morgen, I. Lindau, W.E. Spicer, and J.A. Wilson, J. Vac. Sci. Technol. 21, 154 (1982).

12. W.E. Spicer, J.A. Silberman, J. Morgen, I. Lindau, J.A. Wilson, An-Ban Chen, and A. Sher, Phys. Rev. Lett. 49, 948 (1982).

13. G.D. Davis, W.A. Beck, N.E. Byer, R.R. Daniels, and G. Margaritondo, J. Vac. Sci. Technol. A2, 546 (1984).

14. D.J. Peterman and A. Franciosi, Appl. Phys. Lett. <u>45</u>, 1305 (1984).

15. M.W. Scott, J. Appl. Phys. <u>40</u>, 4077 (1969).

16. A.-B. Chen, A. Sher and W.E. Spicer, J. Vac. Sci. Technol. <u>A1</u>, 1674 (1983).

17. The reduced intensity of the Cd 4d emission at this coverage, the evident line broadening and the emergence of a broad emission feature centered some 12.5 eV below E_F all yield some uncertainty in the estimate of the Cd 4d binding energy change. High resolution photoemission studies of this coverage range are necessary before further discussion of this point.

18. We will avoid using the expression "escape depth" to denote these parameters, since they do not represent the photoelectron escape depth at hν=60 eV as will become clear in the following discussion.

19. These values for the escape depth of 4d photoelectrons from the Cr-Te overlayer are only rough estimates. See, for example, I. Lindau and W.E. Spicer, J. Electron. Spectrosc. <u>3</u>, 49 (1974).

20. V. Solzbach and H.J. Richter, Surf. Sci. <u>97</u>, 191 (1980).

21. G.D. Davis, T.S. Sun, S.P. Buchner, and N.E. Byer, J. Vac. Sci. Technol. <u>19</u>, 472 (1981).

22. M. Schlüter, J.D. Joannopoulos, M.L. Cohen, L. Ley, S.P. Kowalczyk, R.A. Pollak, and D.A. Shirley, Solid State Commun. <u>15</u>, 1007 (1974).

23. Including the ≃3Å Te II layer.

24. See, for example, R.E. Watson and M.L. Perlman, Struct. Bonding <u>24</u>, 82 (1975).

25. P.H. Citrin and G.K. Wertheim, Phys. Rev. B<u>27</u>, 3176 (1983).

26. C.F. Brucker and L.J. Brillson, Thin Solid Films <u>93</u>, 67 (1982).

Figure Captions

Fig. 1 EDC's for the valence band and Hg5d-Cd 4d core emission from
$Hg_{1-x}Cd_xTe(110)$ surfaces obtained by cleaving x=0.22 bulk crystals.

Fig. 2 Valence band and Hg 5d-Cd 4d core emission for the $Hg_{1-x}Cd_xTe(110)$-Cr
interface. The topmost spectra are shown multiplied by a scale
factor of 2.

Fig. 3 Detail of the valence band emission within 9 eV of the Fermi level
E_F for the $Hg_{1-x}Cd_xTe(110)$-Cr interface. Initial Cr deposition
gives rise to increased valence emission within 2 eV of E_F and to
tailing of valence states at E_F. A true Fermi level cut-off,
however, can be seen only for coverages $\Theta>3$.

Fig. 4 Comparison of valence emission from bulk Cr (250Å Cr film on
oxidized Ta) and from the $Hg_{1-x}Cd_xTe$-Cr interface at $\Theta=25$.
The 25Å-coverage interface shows increased emission within 1 eV
below E_F and a 0.2 eV shift to higher binding energy of the
main 3d feature.

Fig. 5 Detail of the Hg 5d and Cd 4d core emission from the $Hg_{1-x}Cd_xTe$-Cr
interface as a function of metal coverage. The vertical dashed lines
indicate the corresponding binding energy as derived from the
deconvolution shown in the top section of Fig. 6. Note the dramatic
increase of the Cd/Hg ratio due to Hg-migration away from the
subsurface layer.

Fig. 6 Top: deconvolution of the experimental lineshape (solid line) in
Hg 5d (dashed line) and Cd 4d (dot-dashed line) contributions for
the clean $Hg_{1-x}Cd_xTe$ surface. The 4d and 5d lineshape were
obtained from HgSe and CdSe samples.
Bottom: semi-logarithmic plot showing the integrated intensity of
the Hg 5d, Cd 4d and Te 4d core emission, normalized to the emission
from the clean surface, as a function of metal coverage. As
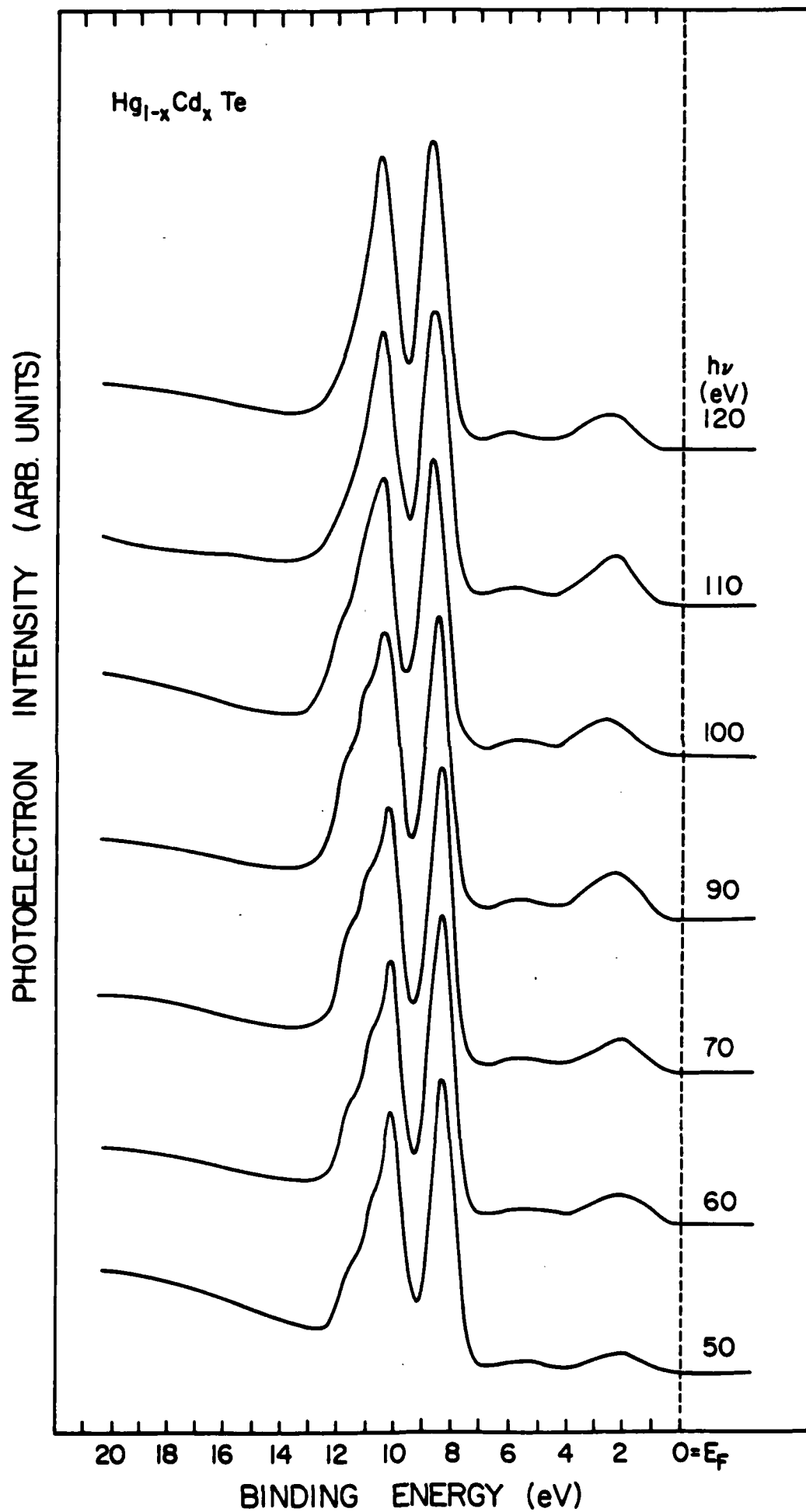discussed in the text, the fast attenuation of the Hg and Cd emission

reflects an exchange reaction in a 10-13 Å subsurface region, where
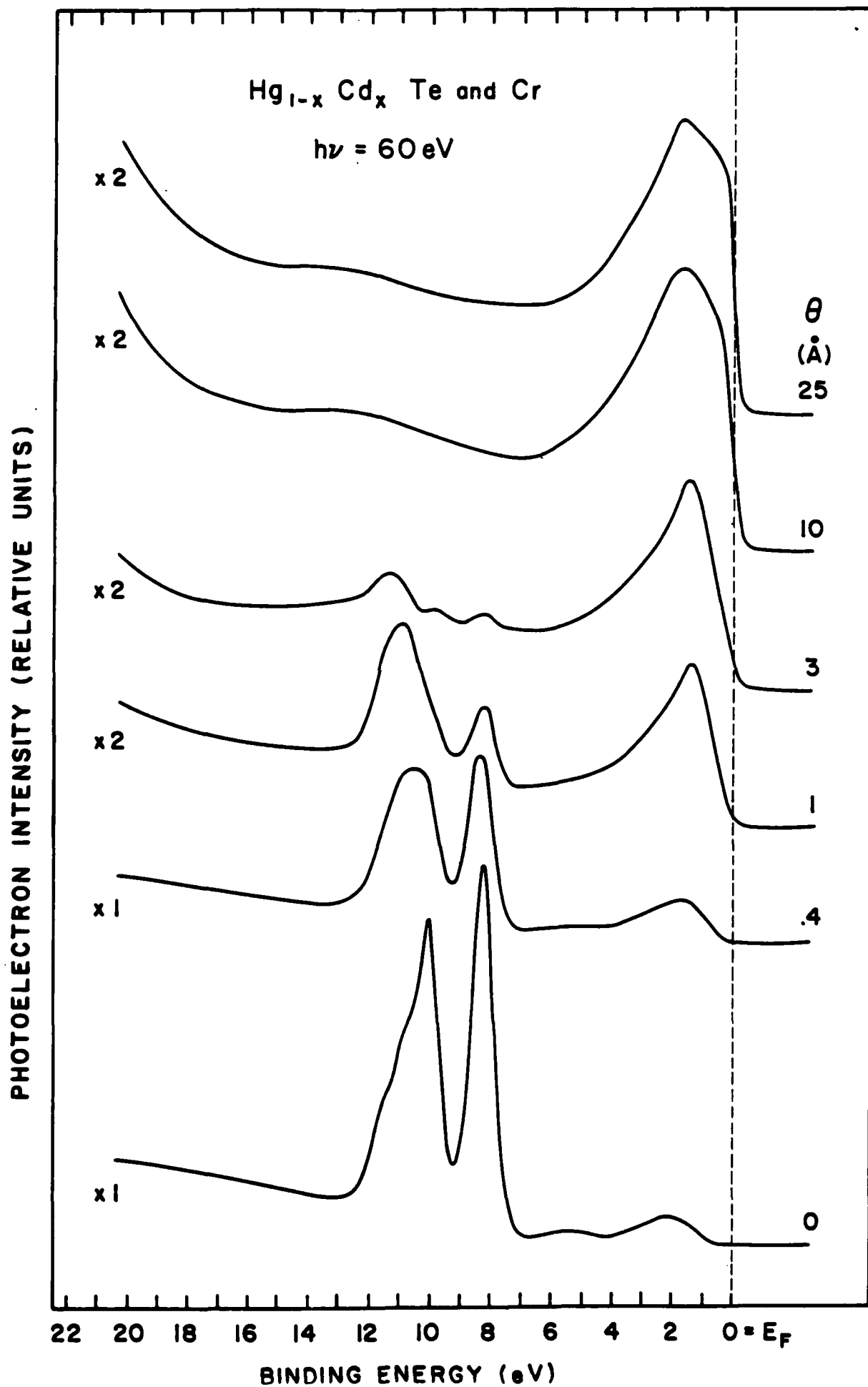all of the Hg atoms and at least 20% of the Cd atoms are replaced by
Cr atoms.

Fig. 7   Te 4d core emission from the $Hg_{1-x}Cd_xTe-Cr$ interface at $h\nu=110$ eV.
Solid line: experiment. Short-dashed line: results of a best
fit using the sum of a Te I subsurface component (long-dashed
line) and a Te II surface component (dot-dashed line). At $h\nu=110$
eV the emission from the Cr 3p cores is negligible for $\Theta<10$.

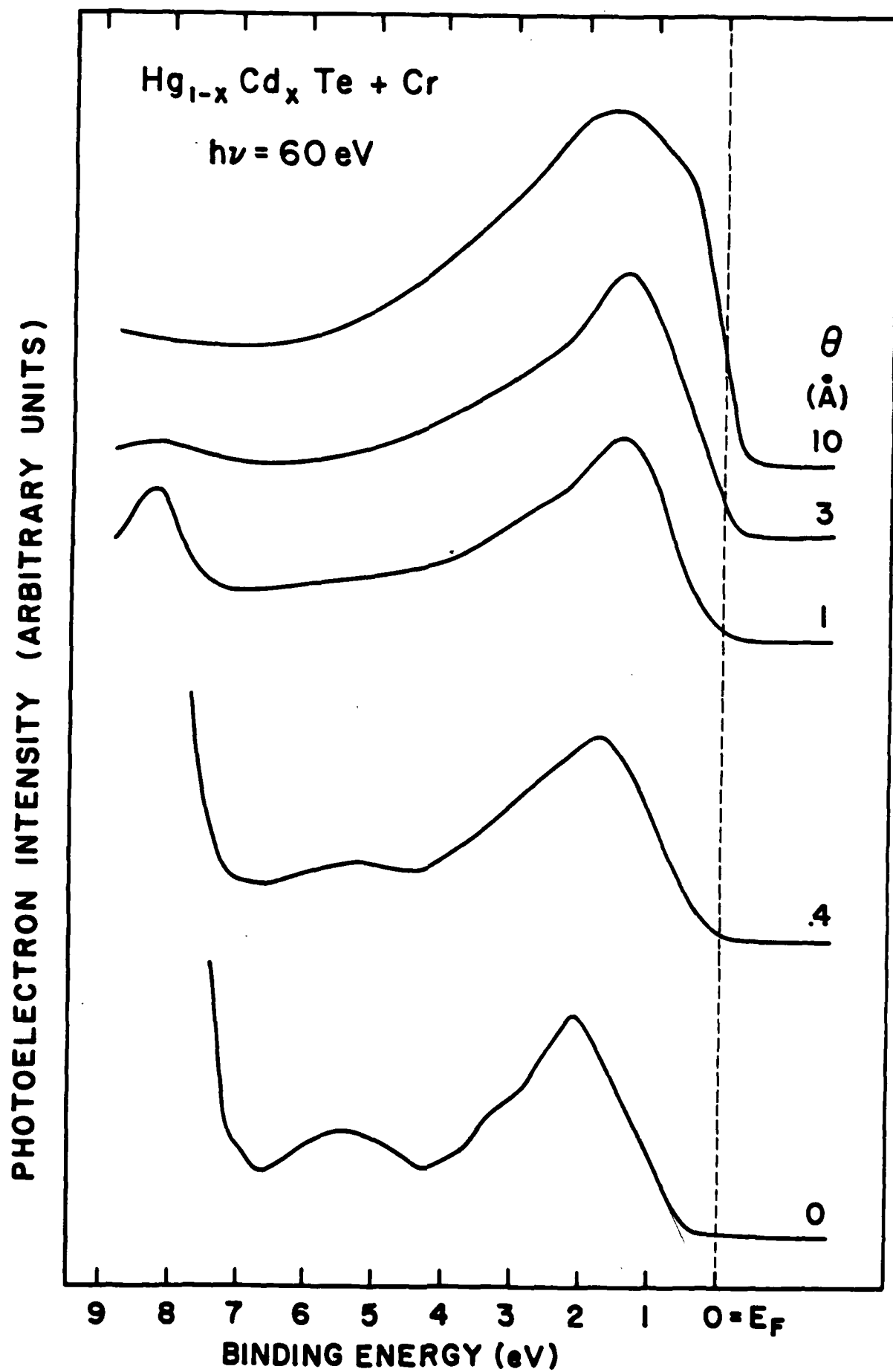Fig. 8   Te 4d core emission from the $Hg_{1-x}Cd_xTe-Cr$ interface at $h\nu=53$ eV.
Solid line: experiment. Short-dashed line: result of a best
fit using the sum of a Te I subsurface component (long-dashed
line), a Te II surface component (dot-dashed line) and a Cr 3p
line (dotted line). The Cr lineshape was obtained from a Cr film
evaporated on an inert substrate. At $h\nu=53$ eV we are near the
photoemission threshold and the Cr signal is of the same order of
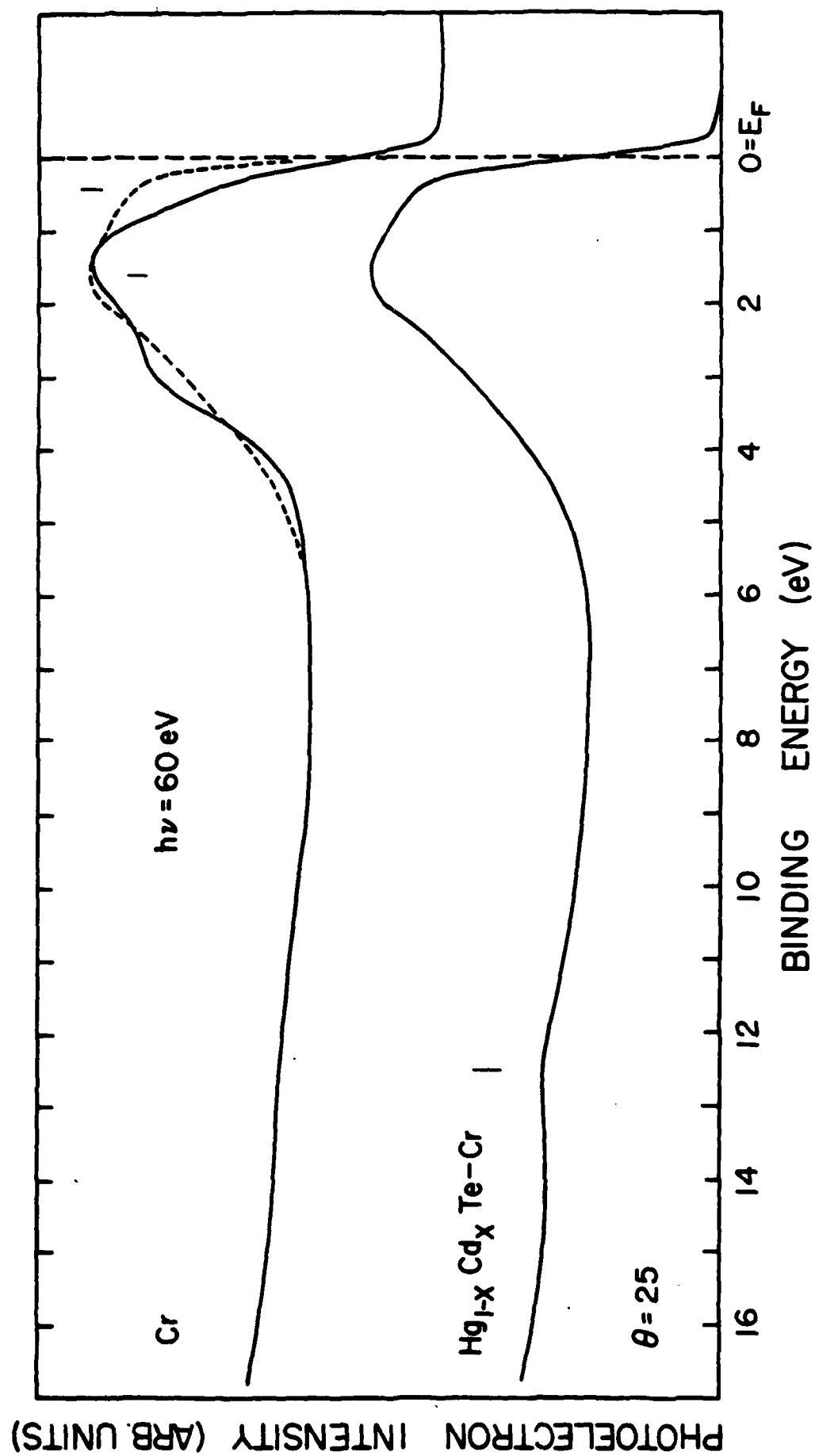magnitude as the Te signal.

Fig. 9   Binding energy of the Cr 3p, Te 4d I and Te 4d II core emission
from the $Hg_{1-x}Cd_xTe-Cr$ interface. The binding energies were
obtained from the deconvolution procedure described in Figs. 7
and 8. The high-coverage saturation values of the Cr 3p and Te 4d
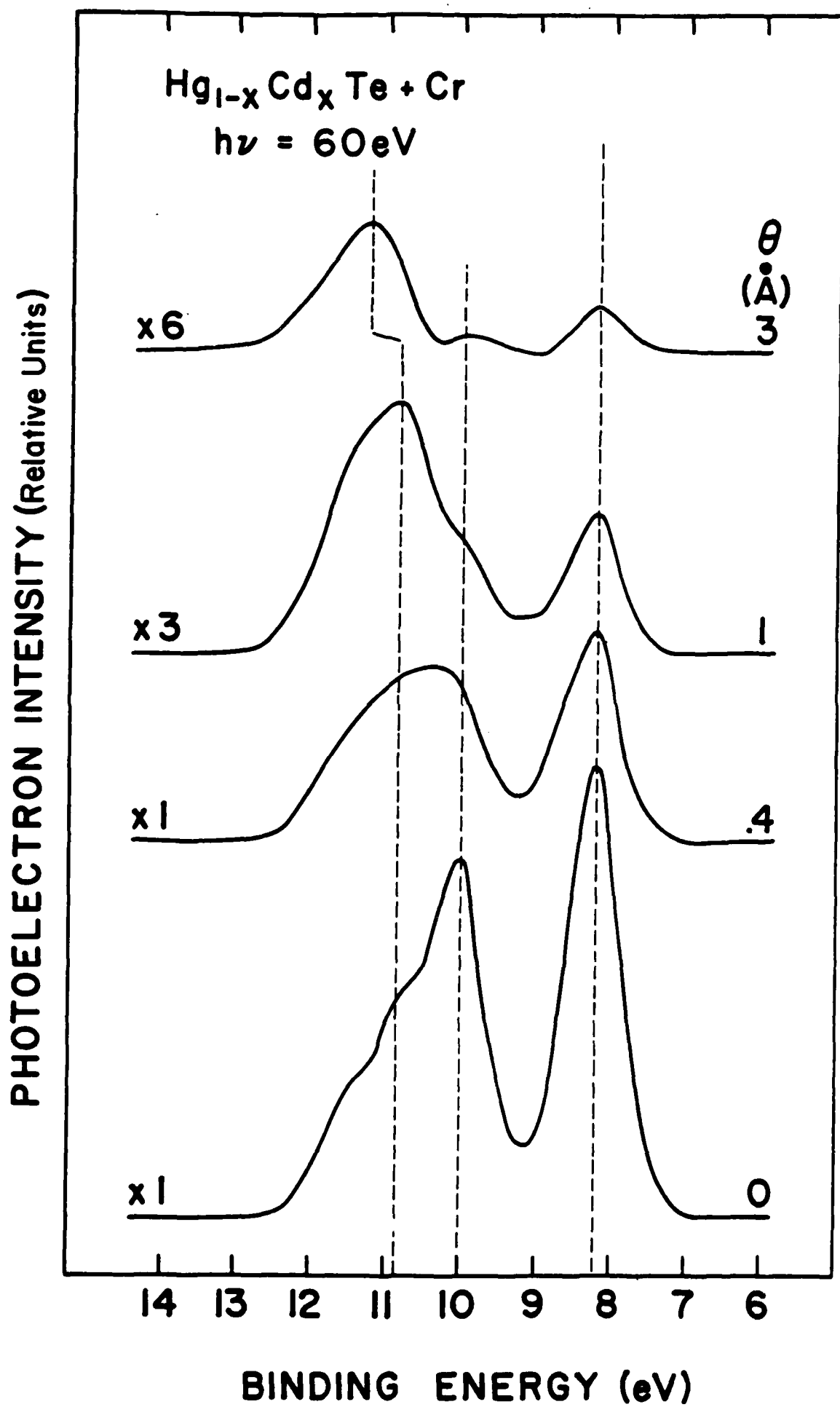II binding energies are close to the elemental values.

Fig. 10 Semilogarithmic plot of the integrated emission intensity of the
Te 4d cores from the $Hg_{1-x}Cd_xTe-Cr$ interface, normalized to the
Te 4d emission from the clean surface. Top: the Te 4d II component
corresponds to dissociated Te released at the surface during the
first interface formation stage. Bottom: the 4d I component
corresponds to Te atoms in the subsurface layer, where the Cr-Hg
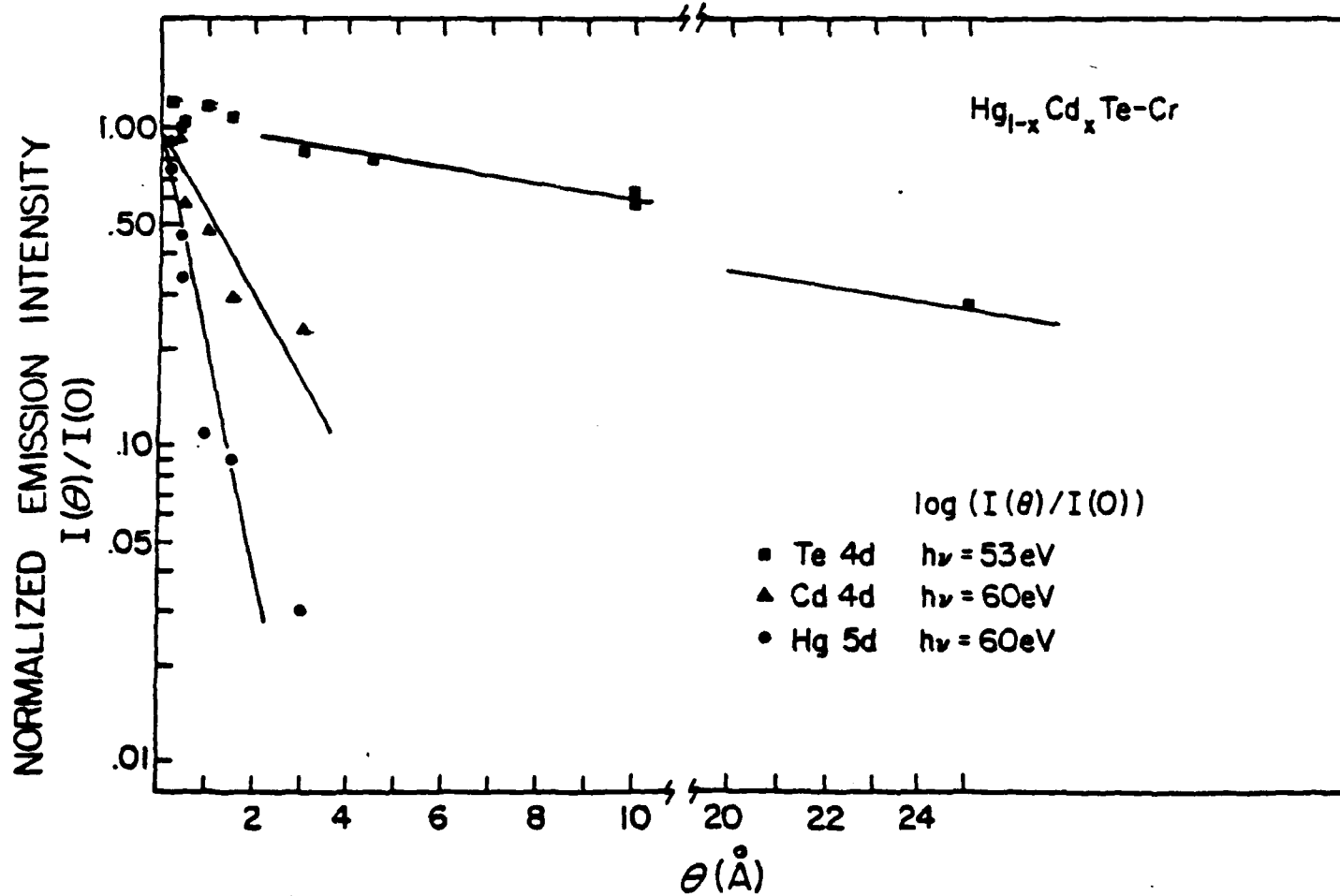(and Cr-Cd) exchange reaction takes place for $\Theta<2$.

$Hg_{1-x}Cd_xTe$

PHOTOELECTRON INTENSITY (ARB. UNITS)

BINDING ENERGY (eV)

$h\nu$ (eV)
120
110
100
90
70
60
50

$0 = E_F$

Hg$_{1-x}$ Cd$_x$ Te and Cr

hν = 60 eV

PHOTOELECTRON INTENSITY (RELATIVE UNITS)

θ (Å)

x2

x2   25

10

x2   3

x2   1

x1   .4

x1   0

22 20 18 16 14 12 10 8 6 4 2 0 = E$_F$

BINDING ENERGY (eV)

Figure showing photoelectron intensity spectra of $Hg_{1-x}Cd_xTe + Cr$ at $h\nu = 60$ eV, plotted as photoelectron intensity (arbitrary units) versus binding energy (eV), for various Cr coverages θ (Å): 10, 3, 1, .4, and 0.

PHOTOELECTRON INTENSITY (ARB UNITS)

BINDING ENERGY (eV)

$h\nu = 60\,eV$

Cr

$Hg_{1-x}Cd_x Te-Cr$

$\theta = 25$

$0 = E_F$

$Hg_{1-x}Cd_xTe + Cr$

$h\nu = 60\,eV$

Hg$_{1-x}$Cd$_x$Te-Cr

hν = 60 eV

Hg 5d

Cd 4d

PHOTOELECTRON INTENSITY (ARB. UNITS)

BINDING ENERGY (eV)

Hg$_{1-x}$Cd$_x$Te-Cr

NORMALIZED EMISSION INTENSITY I(θ)/I(0)

log (I(θ)/I(0))

■ Te 4d   hν = 53 eV

▲ Cd 4d   hν = 60eV

● Hg 5d   hν = 60eV

θ (Å)

Figure axis labels:
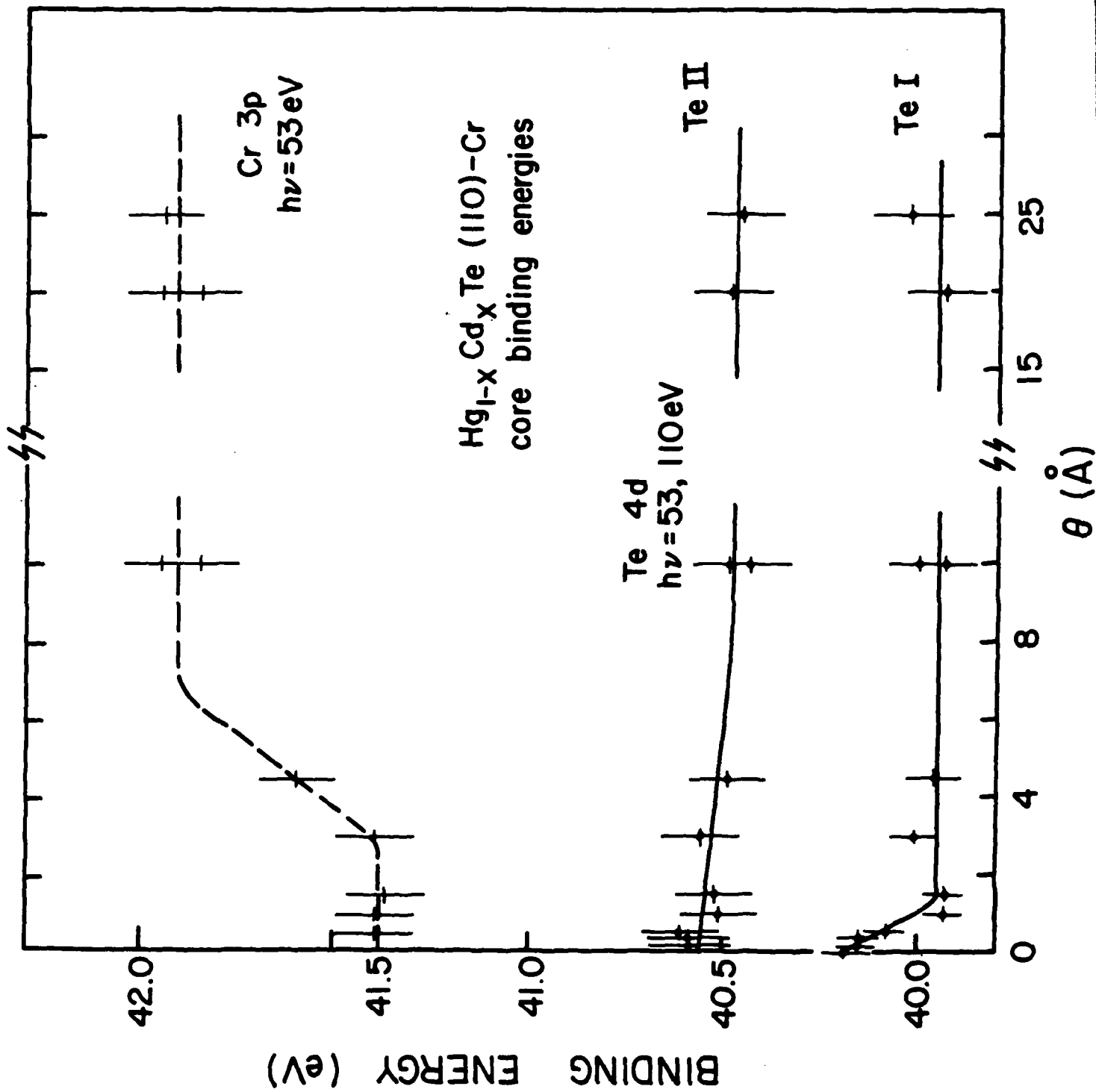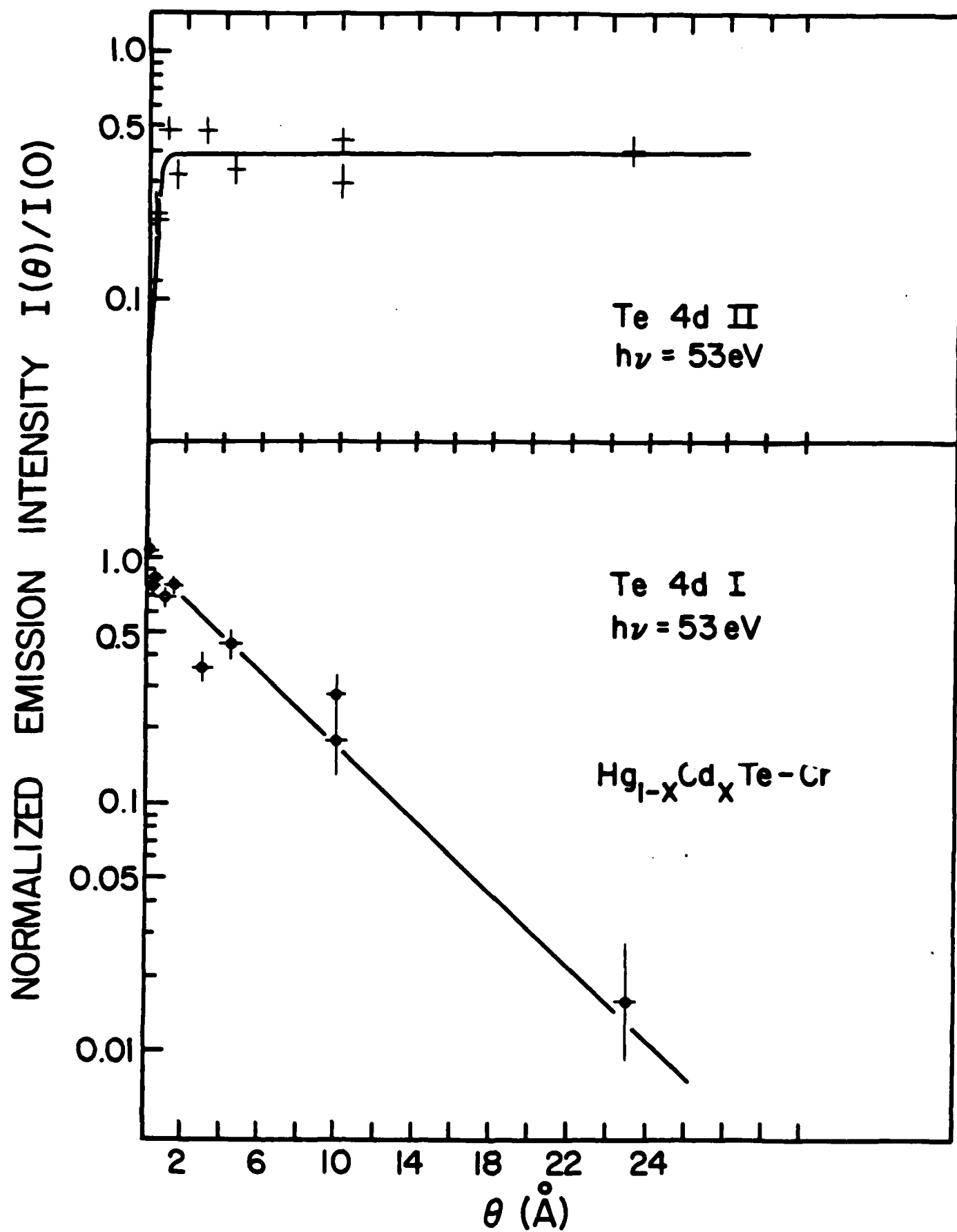PHOTOELECTRON INTENSITY (ARB UNITS)

BINDING ENERGY (eV)

Legend:
Hg$_{1-x}$Cd$_x$Te (110)-Cr
best fit
hν = 110 eV
Te 4d I
Te 4d II

θ (Å): 10, 3, 1.5, 4, 0

Cr 3p
hν=53eV

Hg$_{1-x}$Cd$_x$Te (110)-Cr
core binding energies

Te II

Te I

Te 4d
hν=53, 110eV

θ (Å)

BINDING ENERGY (eV)

42.0   41.5   41.0   40.5   40.0

END

FILMED

12-85

DTIC